Resonant inelastic x-ray scattering study of β-FeSe

M. C. Rahn,[1, *] A. A. Haghighirad,[1] A. J. Princep,[1] K. Kummer,[2] and A. T. Boothroyd[1, †]

[1]*Department of Physics, University of Oxford, Clarendon Laboratory, Oxford, OX1 3PU, United Kingdom*
[2]*European Synchrotron Radiation Facility, BP 220, F-38043 Grenoble Cedex, France*

(Dated: April 25, 2016)

We have performed a resonant inelastic x-ray scattering study on the unconventional superconductor β-FeSe ($T_c \simeq 8\,\mathrm{K}$). The spectra reveal electronic excitations beyond $300\,\mathrm{meV}$. At an energy resolution of $\approx 50\,\mathrm{meV}$ (FWHM), our results allow a distinction of varying trends of dispersion along the $(\pi, 0)$ and (π, π) directions. FeSe is the most metallic system successfully probed by the RIXS technique. Computational simulations of the RIXS process allowing us to relate the present results to existing inelastic neutron studies would be highly desirable.

There has been an intense scientific interest in the magnetic excitation spectra of high temperature superconductors. Both families of cuprate and iron-based superconductors feature magnetic fluctuations extending up to hundreds of meV in energy. Detailed knowledge of these excitations is desirable as they reveal important information about the corresponding ground state, such as the degree and character of electronic correlations [1]. There exists a general consensus that these excitations are at least indirectly involved in the superconducting pairing mechanism. The experimental method of choice to map such magnon dispersions has been inelastic neutron scattering (INS). Modern time of flight neutron spectrometers at are able to reveal important details of the magnetic dispersions, such as the precise propagation vector and the level of itinerancy of the magnetism. One drawback of INS is the weakness of the neutron's interaction with the sample, which necessitates sample masses on the order of several grams. In this regard, over recent years a relevant experimental alternative has emerged in the form of resonant inelastic x-ray scattering (RIXS) at the transition metal L edges. The excitation of electrons from core levels to the magnetically relevant d-orbitals strongly enhances the inelastic scattering of x-rays. Nevertheless, compared with neutron spectroscopy, the RIXS technique retains some inherent limitations: On the one hand, the incident energy is necessarily fixed, which confines the accessible range in momentum space. On the other hand, resolving powers on the order of $E/\mathrm{d}E \approx 14000$ (this study) are needed to discern meV changes in energy of keV photons. However, modern instruments at 3rd generation synchrotrons are now overcoming this limitation. Such has been demonstrated with great success in the case of cuprates, where INS results have been reproduced with impressive accuracy [2, 3].

While iron-based superconductors share some similarities with cuprates, it is their metallic character which has impeded the application of RIXS. Since core electrons can here be excited to the conduction band, most of the spectral weight is transferred to a broad band of fluorescence. This continuous fluorescent background makes it difficult to discern weak paramagnon fluctuations, and thus only few RIXS studies of iron-based superconductors have been successful to date [4, 5]. We here present the results of our study of the iron-chalcogenide β-FeSe (here "FeSe"), using the recently commissioned RIXS end-station of beam line ID32 at the ESRF. FeSe has been of particular interest to the community as it appears to be the most tunable among the family of iron-based superconductors. FeSe is the most metallic compound that has been successfully probed by RIXS. Our results allow a relevant comparison with previously reported INS results: While general features are expected to coincide, the resonant x-ray process differs from the neutron response in that it cannot be calculated analytically. We hope that our results will inspire theoretical developments to tackle this issue of RIXS spectra in metals. As our x-ray spectra cover a much broader energy regime than previous neutron studies, our study determines an upper bound in energy of electronic excitations in FeSe.

High quality single crystals of tetragonal (space group *P4/nmm*) β-FeSe were synthesized using a vapour deposition technique. The compound crystallizes in the form of quadratic platelets with dimensions on the order of $1\,mm^2$ and $\approx 200\,\mu m$ thickness (typical sample mass $< 1\,mg$). Figure 1 illustrates the sample characterization by SQUID magnetometry and laboratory x-ray diffraction. The data confirm a clean onset of the Meissner-Ochsenfeld effect at $T_c = 8\,K$ and a high crystalline quality of these specimen. Exposed to an ambient atmosphere, FeSe crystals tarnish within days. Immediately before RIXS measurement, a top layer was stripped from the sample using an adhesive tape, which revealed a clean, mirror-like surface. The sample was then directly transferred to the UHV system. Inside the sample chamber, the copper sample carrier is transferred to the goniometer, which is connected to the cold finger of a helium flow cryostat via copper braids. Throughout the experiment, the temperature of this sample stage was held at the base temperature of 21 K. The beam size at
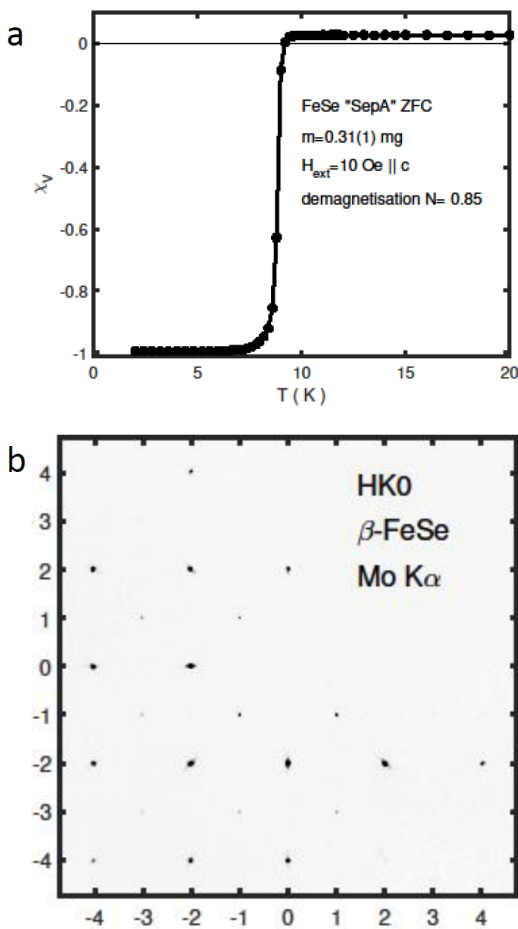
FIG. 1. (a) Volume magnetic susceptibility of β-FeSe single crystal, confirming $T_c = 8$ K. (b) Laboratory single crystal x-ray diffraction of this sample, revealing clear maps of reciprocal space. While the samples exhibit some stacking faults, the in-plane mosaicity is smaller than than the instrumental resolution of the laboratory diffractometer ($\approx 0.6°$).

FIG. 2. (color online) (a) The square iron planes of FeSe are commonly referred to either in the tetragonal ($P4/nmm$, blue), orthorhombic ($Cmma$, red) or "one-Fe" unit cell (green). Throughout this report we use the conventional, "one-Fe" setting. (b) Illustration of reciprocal space with the reciprocal lattice points and outlines of the first Brillouin zones of the three settings marked in colors corresponding to panel (a). In the "one-Fe" convention, the propagation vector of the magnetic fluctuation is $(\pi, 0)$. The regime of reciprocal space accessible to Fe L_3 RIXS is shaded gray. (c) Scattering geometry of the present experiment: The projection of momentum transfer to the (HK0) plane $\mathbf{Q}_\parallel$ is maximised by choosing a large scattering angle 2θ and a low grazing angle δ. We found that we could minimise the quasi-elastic background by choosing a grazing outgoing, rather than grazing incoming beam.

the sample position is $4 \times 60 \, \mu m^2$. After scattering from the sample the outgoing beam is collimated by a mirror, dispersed in energy by a spherical grating and then imaged using a CCD detector placed in the focus of the grating. Due to the thermal expansion of this liquid nitrogen cooled detector, the position of the image on the chip drifts over time. Data is therefore collected in short cycles of 1-5 minutes. Tens of such short scans comprising one measurement are then calibrated and centered with respect to each other using the quasielastic line as reference. The amount of thermal drift over the minimal exposure time required to obtain adequate counting statistics on the quasielastic line is one limiting factor to the energy resolution of the experiment.

With the incident x-ray beam tuned to the Fe L_3 edge ($E_i = 706.8$ eV, $\lambda = 17.54$ Å) we estimate a penetration depth on the order of ≈ 200 nm. The scattering geometry of the experiment is illustrated in Figure 2. The
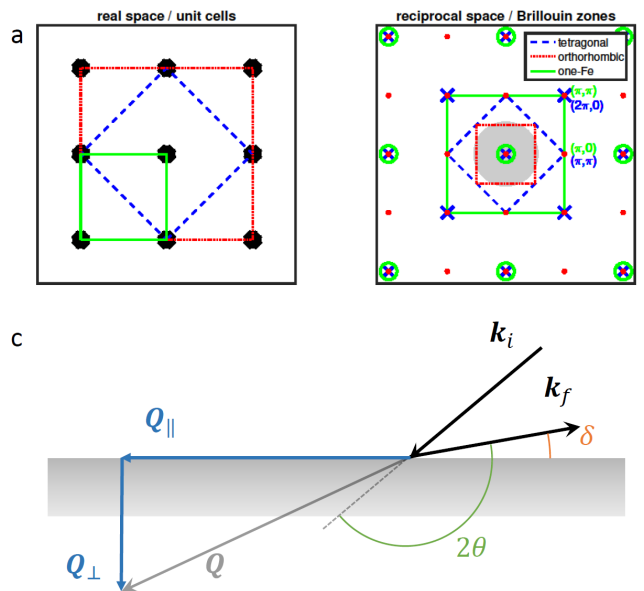
sample was aligned using the specular (001) reflection (accessible by tuning the incident energy to 1.7 keV). As no other Bragg reflection is accessible as a second reference, the azimuth of the sample was aligned by half-cutting the beam with one edge of the quadratic platelet (parallel to a $\langle 100 \rangle$ direction). Spectra were then obtained with the in-plane momentum transfer $\mathbf{Q}_\parallel$ directed along the (100) and (110) directions in the scattering geometry as illustrated in figure 2 c.

Surface deterioration issue. All data were obtained at an incident energy of 707 eV, slightly above the Fe L_3 edge. Electron yield near-edge spectra of the this edge were observed to change with beam irradiation. As shown in Fig. 3, the spectrum of the pristine sample surface is peaked at a 707 meV. After few minutes of irradiation, a hump at ≈ 709 meV begins to gain in in spectral weight and the overall electron yield increases. After several hours of irradiation the feature at ≈ 709 meV saturates. The same characteristics are observed
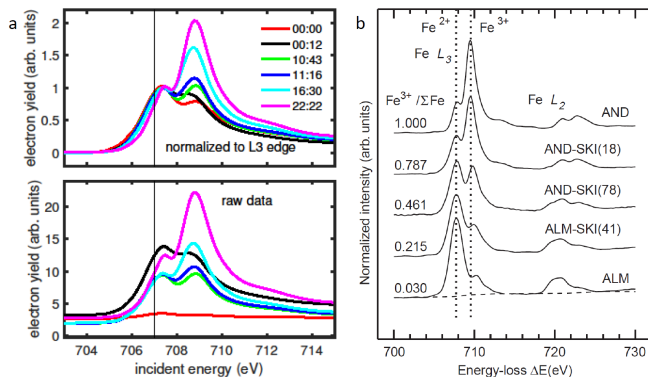
FIG. 3. (color online) Possible deterioration of the sample by irradiation. (a) Electron yield spectra obtained successively at the same position on the sample surface (relative elapsed time indicated as *hh:mm*). The data is shown normalised to the peak at 707 meV (top panel) along with the raw data (bottom panel). (b) Figure taken from [7], illustrating the change in iron L-edge EELS spectra when varying the proportion of Fe^{2+}/Fe^{3+} states, as observed across various mineral samples.
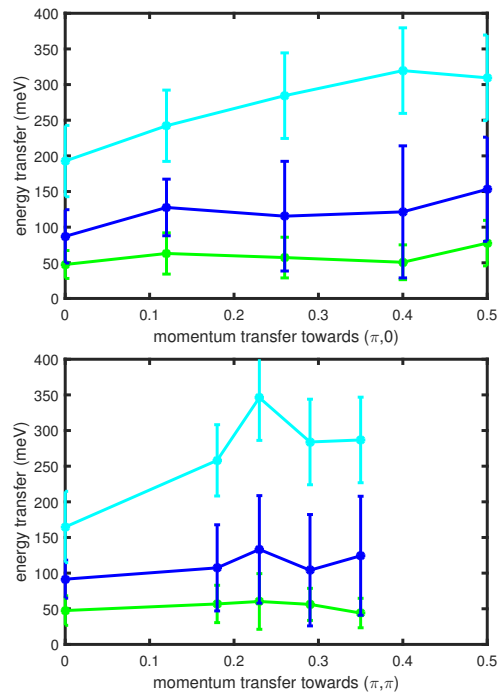

FIG. 4. (color online) Dispersion of electronic excitations, as phenomenologically modelled by three gaussians in figs. 6 and 8. Characteristics along (1,0) (top panel) and (1,1) (bottom panel). Plot colors correspond to the fits represented in figures 8 and 6, respectively.

in both electron yield and x-ray absorption spectra. Moving the beam to a different position on the sample surface readily restores the original features. The iron L_3 characteristics of fluorides, oxides and covalent compounds have recently been reviewed by Miedema *et al.* [6]. Across various compounds, it is seen that the second peak (2 meV above the first L_3 edge feature) is a general feature of the Fe^3+ oxidation state. The variation of electron energy loss spectroscopy (EELS) characteristics between minerals of varying Fe^{3+}/Fe^{2+} proportion has beeen studied by van Aken *et al.* [7] (reproduced in Figure 3). This implies that some of the sample volume probed in this experiment may have been altered by the beam, possibly locally forming an Fe^{3+} compound such as Fe_2O_3 or Fe_2Se_3.

As a minimal phenomenological model for the fluorescent background and quasielastic scattering, a stretched exponential and a gaussian peak centered at $E = 0$ were fitted and subtracted from each RIXS spectrum:

$$f(E) = A_1 \, 0.5^{(2\,E/\delta)^2} + A_2 \, \exp^{-\alpha(E-E_0)} \qquad (1)$$

With the scale factors (A_1, A_2), the FWHM of the gaussian peak (δ), as well as the position and "decay constant" of the fluorescent background (E_0, α) as fit parameters. More elaborate models of the fluorescence (*e.g.*, involving a step-function at $E = 0$ or polynomial instead of exponential functions) were tested but produced only marginally different results. To ensure a fit to the desired part of the spectral weight the regime with significant inelastic signal (from -400 meV to -15 meV energy transfer) was excluded from the fit. Notably, the

FWHM of the fitted gaussian peak was *not* constrained to the width of the elastic reference measurement. Therefore, the remaining difference signal does not represent the full excitation spectrum but may be overcompensated for low-energy excitations adding to the quasielastic line. This applies in particular to those data obtained at a scattering angle $2\theta = 90$: In this setting, quasielastic scattering is extinct, yet a significant gaussian contribution was observed at $E = 0$. Moving away in small steps from the $2\theta = 90$ condition revealed that this low energy inelastic intensity is indeed centered at the position of the then emerging elastic line.
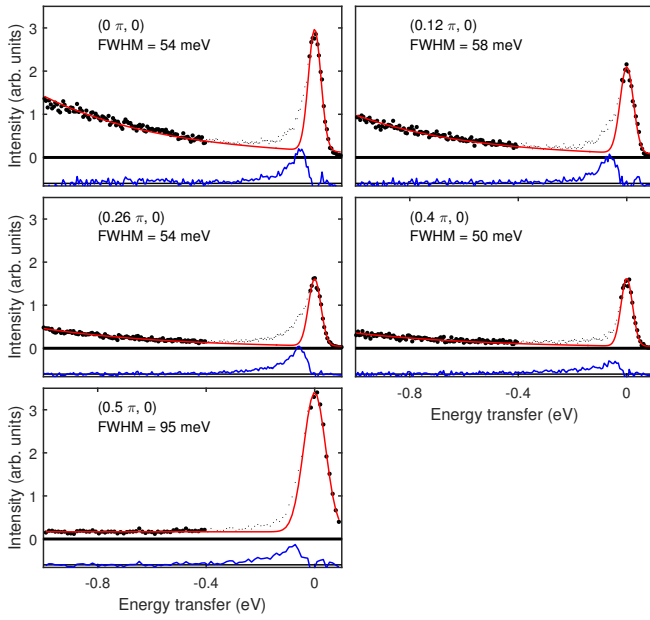
FIG. 5. (color online) RIXS spectra with the momentum transfer directed along the (1,0) direction. Sections (thick markers) of the data (black) were approximated by eq. 1. The resulting fits (red), difference signal (blue) and FWHM of the quasielastic line are indicated for each momentum transfer.
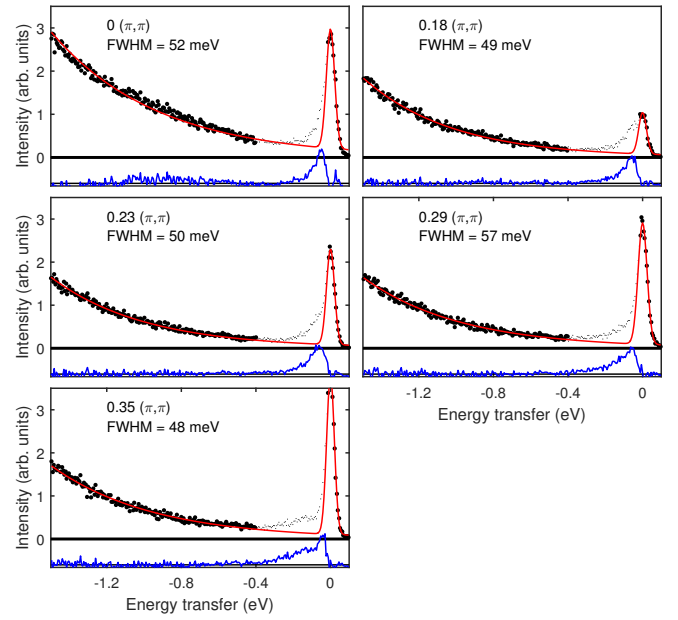
FIG. 7. (color online) RIXS spectra with the momentum transfer directed along the (1,1) direction. Sections (thick markers) of the data (black) were approximated by eq. 1. The resulting fits (red), difference signal (blue) and FWHM of the quasielastic line are indicated for each momentum transfer.
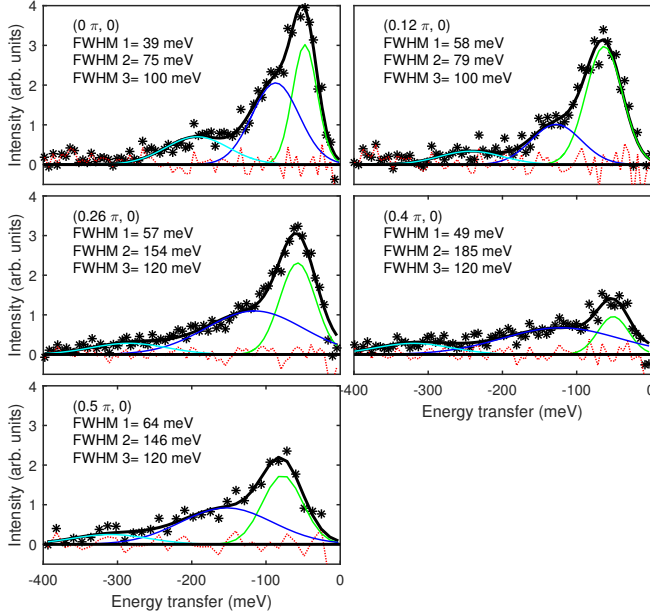
FIG. 6. (color online) High energy RIXS excitations with the momentum transfer directed along the (1,0) direction. The difference signal (black markers) was obtained as demonstrated in figure 5. At least three components (green, blue, cyan gaussian peaks) are necessary to phenomenologically model the resulting spectra.
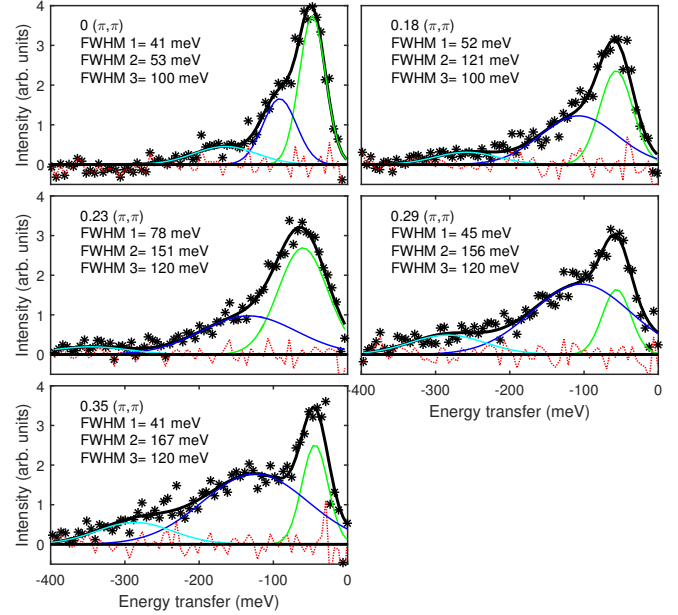
FIG. 8. (color online) High energy RIXS excitations with the momentum transfer directed along the (1,1) direction. The difference signal (black markers) was obtained as demonstrated in figure 7. At least three components (green, blue, cyan gaussian peaks) are necessary to phenomenologically model the resulting spectra.
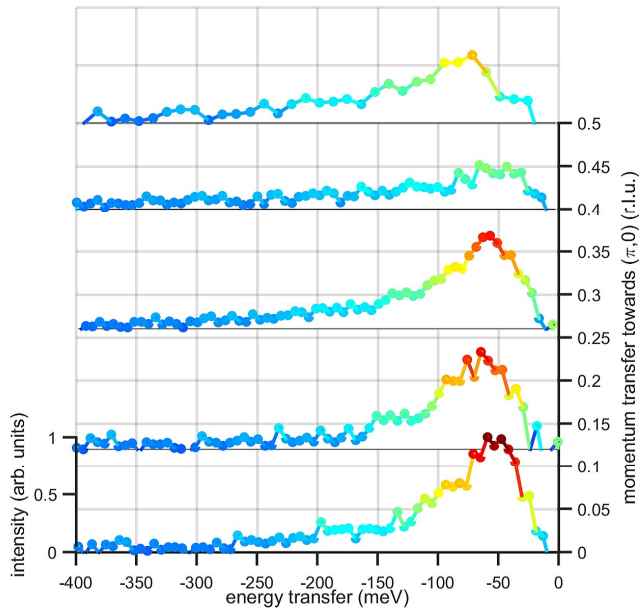
FIG. 9. (color online) RIXS spectra with momentum transfer along the (1,0) direction (data as in figure 6) represented in a waterfall plot for better comparison.
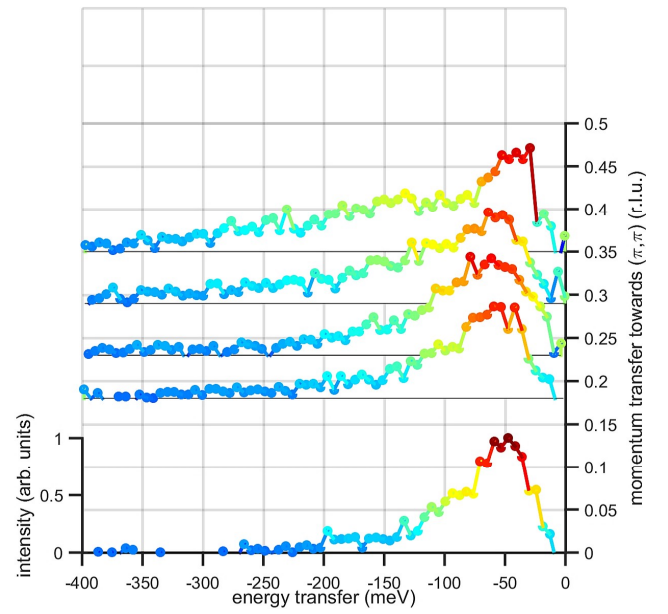

FIG. 10. (color online) RIXS spectra with momentum transfer along the (1,1) direction (data as in figure 8) represented in a waterfall plot for better comparison.

The results are summarised in figure 5 ($\mathbf{Q}_\parallel \parallel (1,0)$) and 7 ($\mathbf{Q}_\parallel \parallel (1,1)$). The corresponding difference signals are further detailed in figures 6 and 8. As a guide to the eye, these spectra were phenomenologically fitted by three gaussian peaks, highlighting significant structure in these lines. It should be noted that phonon excitations in FeSe are confined to energies below $40\,\mathrm{meV}$ [8]. The spectral weight which is seen to disperse beyond $300\,\mathrm{meV}$ must therefore be attributed to different electronic or magnetic origins and would be in good agreement with the high-energy paramagnon bands observed in neutron spectroscopy [8, 9]. For better comparison, the data of figs. 6 and 8 is represented in form of waterfall plots in figs. 9 and 10. Lastly, the dispersion of the phenomenological fits to the high energy excitation is plotted in figure 4, where the width of the errorbars reflects the FWHM of the corresponding gaussian peaks in figures 6 and 8. As an actual physical model is lacking at this point, these dispersions are merely intended as a rough visualisation of the data.

---

* marein.rahn@physics.ox.ac.uk

† a.boothroyd@physics.ox.ac.uk

[1] P. Dai, Rev. Mod. Phys. **87**, 855 (2015).
[2] L. Braicovich, L. J. P. Ament, V. Bisogni, F. Forte, C. Aruta, G. Balestrino, N. B. Brookes, G. M. De Luca, P. G. Medaglia, F. M. Granozio, M. Radovic, M. Salluzzo, J. van den Brink, and G. Ghiringhelli, Phys. Rev. Lett. **102**, 167401 (2009).
[3] M. Le Tacon, M. Minola, D. C. Peets, M. Moretti Sala, S. Blanco-Canosa, V. Hinkov, R. Liang, D. A. Bonn, W. N. Hardy, C. T. Lin, T. Schmitt, L. Braicovich, G. Ghiringhelli, and B. Keimer, Phys. Rev. B **88**, 020501 (2013).
[4] J. N. Hancock, R. Viennois, D. van der Marel, H. M. Rønnow, M. Guarise, P.-H. Lin, M. Grioni, M. Moretti Sala, G. Ghiringhelli, V. N. Strocov, J. Schlappa, and T. Schmitt, Phys. Rev. B **82**, 020513 (2010).
[5] K.-J. Zhou, Y.-B. Huang, C. Monney, X. Dai, V. N. Strocov, N.-L. Wang, Z.-G. Chen, C. Zhang, P. Dai, L. Patthey, J. van den Brink, H. Ding, and T. Schmitt, Nat Commun **4**, 1470 (2013).
[6] P. S. Miedema and F. M. F. de Groot, Journal of Electron Spectroscopy and Related Phenomena , 32 (2013).
[7] P. A. van Aken, B. Liebscher, and V. J. Styrsa, Phys Chem Minerals **25**, 323 (1998).
[8] M. C. Rahn, R. A. Ewings, S. J. Sedlmaier, S. J. Clarke, and A. T. Boothroyd, Phys. Rev. B **91**, 180501 (2015).
[9] F. Wang, S. Kivelson, and D.-H. Lee, arXiv:1501.00844 (unpublished) (2015).